

A STED Microscope Designed for Routine Biomedical Applications

Frederik Görlitz¹, Patrick Hoyer¹, Henning J. Falk¹,
Lars Kastrop², Johann Engelhardt¹, and Stefan W. Hell^{1, 2, *}

(Invited Paper)

Abstract—We present a multi-color STED fluorescence microscope providing far-field optical resolution down to 20 nm for biomedical research. The optical design comprises fiber lasers, beam scanners, and a set of active and passive polarizing elements that cooperatively yield an optically robust system for routinely imaging samples at subdiffraction length scales.

1. INTRODUCTION

Far-field optical microscopy is the most widely employed microscopy modality in the basic life sciences. Relying on freely propagating light, it gives largely non-destructive access to the interior of living cells and sub-surface tissue layers and, in combination with fluorescence tagging, it also provides unsurpassed molecular specificity and sensitivity. However, the spatial resolution of traditional fluorescence microscopy is limited by diffraction to 200–350 nm, which is why most subcellular features cannot be discerned with this widely used approach.

The development of stimulated emission depletion (STED) fluorescence microscopy [1–3], that took place at the turn of this century, demonstrated that the limiting role of diffraction can be overcome and nanosized features discerned with freely propagating light and conventional lenses. The decisive difference between STED and the traditional microscopy approaches is that the traditional ones discern the tiny features in the sample by the phenomenon of focusing. In simple terms, adjacent features are discerned by sharply focusing the light that comes from, or falls on the features to be separated. Separation by focusing is clearly limited by diffraction due to the minimal spot size that can be created by a lens. In contrast, STED microscopy discerns neighboring features by ensuring that the molecules defining these features occupy different molecular states when scrutinized for optical detection, e.g., illuminated by the same diffraction pattern of excitation light. Discerning by states is clearly not limited by diffraction. Selecting two distinguishable states and a suitable transition is enough to literally make the decisive difference (between the features) and eliminate the limiting role of diffraction [4].

In STED microscopy, the molecular states employed for separation are the excited fluorescent state of the fluorophore and its ground state. The pertinent state transition is that of stimulated emission, i.e., the optically induced transition from the excited to the ground state. To get the fluorophores of adjacent features sequentially into these different states, STED microscopy employs the so-called STED beam, whose wavelength and intensity are chosen such that stimulated emission is ensured. Concretely, the wavelength λ is centered in the long-wavelength part of the emission spectrum of the fluorophore, whereas the intensity is large enough to make the transition from the fluorescent state down to the ground state nearly certain at the given molecular cross-section of interaction. The STED beam thus prevents the occupation of the fluorescent state, even when the molecules are illuminated with excitation light. Additionally, the STED beam is designed to feature one or more intensity minima in

Received 27 April 2014, Accepted 28 May 2014, Scheduled 15 June 2014

* Corresponding author: Stefan W. Hell (stefan.hell@mpibpc.mpg.de).

¹ German Cancer Research Center (DKFZ), BioQuant (INF 267), Im Neuenheimer Feld 280, Heidelberg 69120, Germany.

² Department of NanoBiophotonics, Max Planck Institute for Biophysical Chemistry, Am Fassberg 11, Göttingen 37077, Germany.

the focal plane, so that all molecules are effectively kept in the ground state, except those that happen to be located at the minimum and its immediate proximity $\Delta r \ll \lambda/2$ of subdiffraction extent. Thus, stimulated emission creates a highly localized and well defined state difference in the sample, providing molecular separation. When the STED beam is co-aligned with the excitation beam and translated across the object, molecules that are just slightly further apart from each other than Δr cannot reside in the same state at the same time; they are forced to occupy the fluorescent state consecutively. As a result, they can be distinguished.

In good approximation, the resolution of the STED imaging modality is given by

$$\Delta r \approx C\lambda / \left(2NA\sqrt{1 + I/I_s} \right) \quad (1)$$

NA is the numerical aperture of the lens, I the peak intensity bordering the minimum, and I_s a fluorophore-characteristic measure of the minimal intensity that is required to make the state transition probable enough for discerning the molecules by states; it can be arbitrarily chosen within a range. Oftentimes it is chosen as the value at which the transition probability is 50%. For completeness, we note that the parameter C is co-determined by the actual choice of I_s , and for small values I/I_s , the parameter C also depends on the excitation wavelength.

Although stimulated emission and the involved states are very basic, making STED microscopy widely applicable, there are also other molecular state pairs and transitions that can be harnessed for making molecules discernible. Examples comprise transferring the molecules to a transient dark state [5], optical transfers between two distinguishable fluorophore isomers (e.g., ‘photoswitching’ fluorophores), and others [6]. Separating features by states rather than by waves, and more specifically, preventing the molecules of neighboring features to occupy their fluorescent state at the same time, is also the basis of the stochastic nanoscopy approaches that detect and localize individual molecules (PALM/STORM) [7–9]. The same applies to methods that evaluate higher order emission correlations of simultaneously emitting fluorophores (SOFI) [10], and in fact, to all current fluorescence ‘superresolution’ approaches of practical relevance. If one removed the physical element of making adjacent features transiently distinct by a molecular state transition, none of these concepts would work [11]. This element is also responsible for the important fact that conceptually, all these approaches can reach resolution down to the size of a molecule.

STED microscopy has so far been mostly implemented in confocalized single-beam scanning setups using a conventionally focused excitation beam that is co-aligned with a doughnut-shaped beam for STED. Scanning the co-aligned beams across the sample automatically produces the state transitions required for feature separation and signaling, rendering the subdiffraction image as a result. The resolution can be adjusted by tuning the intensity I at the doughnut crest, as indicated in the above equation. Both pulsed and continuous wave (CW) STED lasers can be used. Whereas CW lasers are available in many wavelengths and do not necessitate synchronization between the processes of excitation and STED, they require higher average power to reach the same resolution value, as compared to standard 80 MHz pulsed lasers [12]. Therefore, although CW lasers are in common use — most notably in commercial STED microscopes — pulsed laser sources are preferable for attaining high resolution. Since they minimize timing jitter, spurious multi-photon excitation, and photobleaching, STED pulse durations of 0.3–1 ns have proven particularly advantageous.

However, since initial versions of pulsed STED microscopy were realized with mode-locked Ti:Sapphire lasers that are followed by complex optical units for pulse stretching, wavelength and wavefront modification, the realization of pulsed-mode STED microscopy has occasionally been considered demanding. Additionally, co-aligning the beams, controlling the pulse timing, and producing the doughnut-shaped beam called for optical subunits that added complexity to the system. Doughnut production and the scanning of the beams also called for dedicated optical planes that are conjugate to the entrance pupil of the objective lens and accessible, making the system bulky. Multiple color detection also required a set of exchangeable dichroic mirrors.

Although a number of isolated optical solutions have been proposed to address these issues, the question still remained whether a design can be evolved that meets all these demands at a high level of performance. Here we describe an optical STED microscopy design that synergistically combines these individual solutions, yielding a virtually alignment-free and affordable STED fluorescence ‘nanoscope’

that allows the detection of multiple markers in routine biomedical applications with a resolution down to 20 nm.

2. EXPERIMENTAL SETUP

Our STED system uses a low power pulsed supercontinuum laser source (WhiteLase SC450-PP-HE, Fianium, Southampton, UK) for excitation at virtually any optical wavelength. After removal of the IR part of the supercontinuum spectrum using a 760 nm short pass filter, the desired excitation wavelength is selected using an acousto-optic tunable filter (AOTF, PCAOM-VIS, Crystal Technologies, Palo Alto, USA). The beam passes the AOTF three times in order to suppress the undesired wavelength range of the supercontinuum spectrum; the triple pass suppresses 1000 times better than a regular single pass (see Figure A1) [13]. The STED laser is a frequency-doubled pulsed fiber laser (PFL1-1000-775, MPB Communications, Montreal, Canada) providing 1 ns pulses of up to 30 nJ pulse energy at a wavelength of 775 nm. The STED laser can be triggered electronically over a wide frequency range (25–40 MHz) which greatly simplifies the synchronization of the excitation and STED pulses. In our case, the STED laser is triggered by the pulsed supercontinuum laser operating at 38 MHz. STED beams at 775 nm wavelength are quite efficient for STED of fluorophores having peak emissions between 600 nm and 700 nm, a fact which can be used for multicolor recordings using a single-wavelength STED beam [14]. A notable advantage of a single STED beam approach is that the region in which the different fluorophores can assume the signaling state is defined by the very same doughnut. Mislocalizations due to chromatic aberrations are thus excluded.

The optical design of our setup is sketched in Figure 1. Both laser beams are combined and jointly coupled into a polarization maintaining (PM) optical fiber. After collimation, a directional beam splitter (DBS) as described in Subsection 2.3 directs the laser light to the microscope. Beam scanning is implemented with a Quadscanner (see Subsection 2.2) mounted on the side port of the microscope body (DMI6000 CS, Leica, Wetzlar, Germany). An easySTED waveplate (WP, see Subsection 2.1) mounted

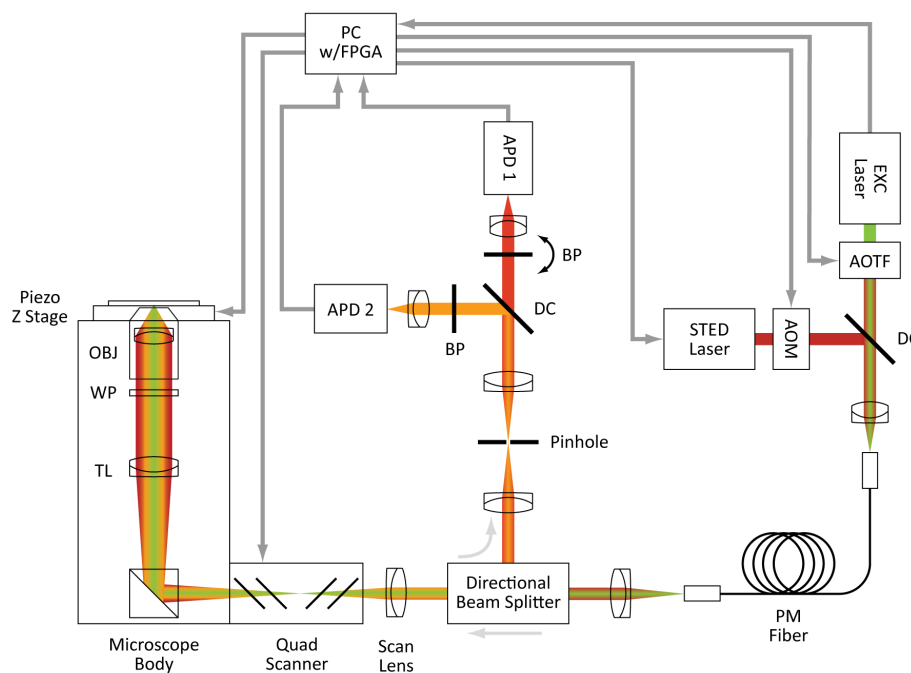


Figure 1. Schematic design of the STED microscope. Abbreviations: objective lens (OBJ), easySTED waveplate (WP), tube lens (TL), dichroic beamsplitter (DC), band pass filter (BP), avalanche photo diodes (APD1, APD2), acousto-optic modulator (AOM), acousto-optic tunable filter (AOTF), computer with FPGA based electronics board (PC w/FPGA).

between the tube lens (TL) and the objective lens (OBJ) transforms the STED beam into a doughnut at the sample, while leaving the other beams focused. The fluorescence light emerging from the sample is collected by the same objective lens, descanned, and directed towards the detection system by the DBS. The detection system contains a confocal pinhole, after which the fluorescence is split by a dichroic beam splitter (DC) into two wavelength bands and detected with two avalanche photodiodes (APD1, APD2, SPCM-AQRH-13, Excelitas Technologies Corp., Waltham, MA, USA). Bandpass filters (BP) in front of the detectors suppress residual laser light.

To minimize the thermal drift of the sample (which in common research-grade microscopes amounts to ~ 100 nm per few minutes), a low weight sample stage was designed and mounted directly onto the objective lens (Figure A2). Our design reduces the overall mechanical path between the sample and the objective lens, and due to its low inertia, is largely immune against external vibrations. We found that the sample drift measured during a 3.5 min interval is reduced to < 13.5 nm in the x, y -direction and 140 nm in the z -direction when the environmental temperature variation is $< 2^\circ\text{C}$.

All functions of the STED microscope are controlled by a field-programmable gate array (FPGA) based PC board (PCIe-7852R, National Instruments, Austin, TX, USA) which is operated with a custom program and a graphical user interface implemented in LabVIEW (National Instruments). Besides controlling the galvanometer scanners and the piezo stage for focus control, the FPGA adjusts the timing between the excitation and the STED laser pulses, and comprises a photon counting scheme with temporally gated detection [15,16]. For these purposes, programmable delay lines inside the Virtex V type FPGA chip are used which provide a time resolution of 80 ps. In the following sections, we shall describe the key elements of our setup in detail.

2.1. EasySTED Phase Plate

The wavefront modifying easySTED phase plate [17,18] reduces the demands for optical alignment significantly. Because it is placed in the common excitation and STED beam path, both laser beams can be coupled into a microscope through a single optical fiber. The easySTED wave plate is a birefringent phase retarding element consisting of four segments of different orientation (Figure 2) to the effect that it leaves the polarization of the excitation light mostly unchanged, while the polarization of the STED beam is modified such that it renders a focal doughnut [17,18] (see Figure 2). The chromatic dependence of the wave plate makes the excitation intensity spot somewhat larger and triangularly shaped at wavelengths > 50 nm away from the design wavelength. This may slightly increase photobleaching because fluorophores located at the periphery of the excitation spot are unnecessarily excited. On the

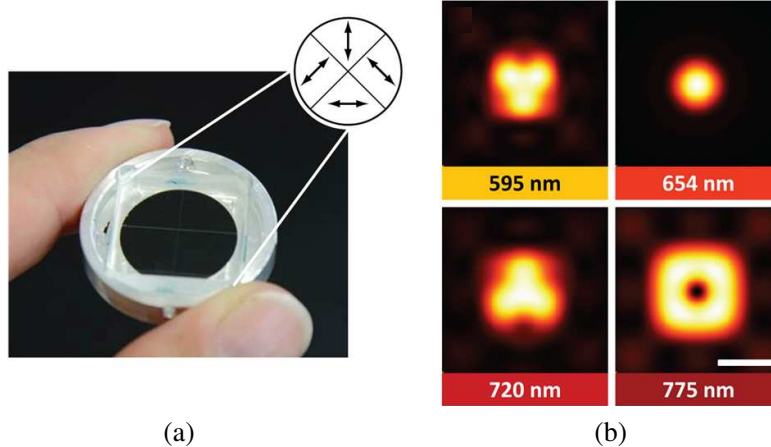


Figure 2. (a) Photograph and schematic (inset) of the easySTED wave plate. The arrows indicate the orientation of the fast axes in the segmented wave plate. (b) Wavelength dependence of the wave plate: at 654 nm (the excitation wavelength), the retardation is 3λ and a perfect diffraction limited spot is formed whereas, at 775 nm (the STED wavelength), the retardation is 2.5λ and a doughnut shape is formed. The spot shape is largely conserved between 595 nm and 720 nm. Scale bar: 500 nm.

other hand, since the coordinates of fluorescence emission are dictated by the position of the doughnut, the triangular shape of the excitation spot does not become manifested in the images.

The wavelength dependence of the easySTED phase plate means that STED lasers with spectral bandwidth of a few nanometers or larger, such as a Titanium:Sapphire laser, are not compatible with the easySTED approach, because the doughnut minimum is filled up quickly. Since it has a < 1 nm linewidth, our 775 nm pulsed fiber laser harmonizes perfectly well with the easySTED phase plate. At the same time, this laser is less expensive and provides the right pulse duration (1 ns). Moreover, it can be triggered, which greatly simplifies synchronization with pulsed excitation lasers. Thus, alignment is reduced to a simple coupling of multiple laser lines into a singlemode fiber. Note that the easySTED phase plate can be adjusted to the desired wavelength by changing the thickness of its material or the refractive index.

2.2. The Quadscanner

In contrast to conventional scanning arrangements, the Quadscanner (Figure 3) is placed in an intermediate image plane of the microscope, rather than in a plane that is conjugate to the entrance pupil of the objective lens [19]. In this design, the collimated laser beam remains stationary all the way to the side port of the microscope stand making large and complex scan lenses obsolete. An achromatic lens is sufficient for the collimated millimeter-sized beam. For each scan direction, a pair of galvanometers translates the focus in the intermediate image plane. The lateral as well as the axial position of the pivot points of the beam can be controlled by adjusting the ratio of the scan angles of each galvanometer pair. In this design, neither the scanning mirrors nor the easySTED waveplate need to be placed in planes that are conjugate to the entrance pupil, making optical relays redundant and the system virtually alignment-free.

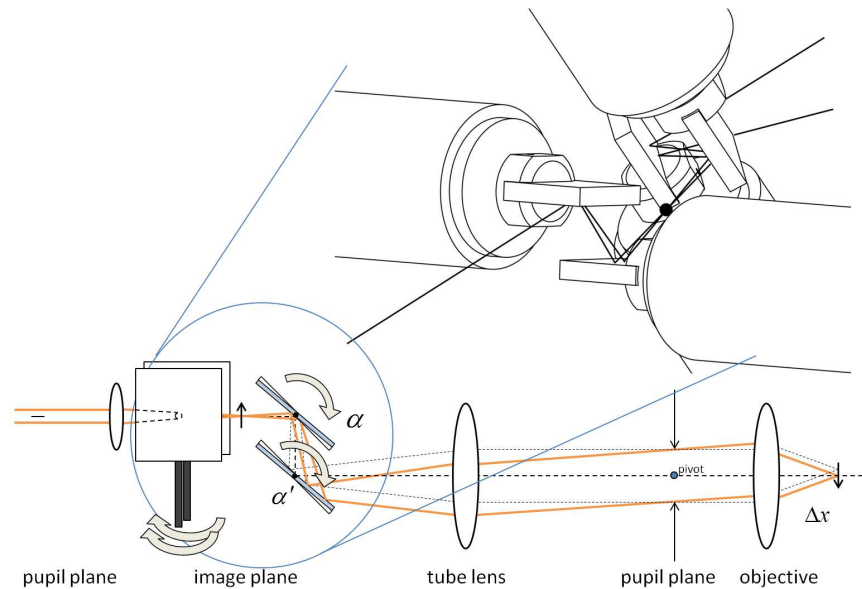


Figure 3. Schematic of the Quadscanner. In contrast to conventional scanners which are placed in a pupil plane of the beam path, the Quadscanner is placed in an intermediate image plane. Scanning is performed by translating the laser beam rather than tilting it.

The maximum field of view rendered by the Quadscanner is defined by the mirror sizes of the galvanometers; it amounts to $80 \times 80 \mu\text{m}$ in the current design using a 100x objective. The electronic resolution (16 bit) used here allows addressing a raster of nominally 1.5 nm in the object plane. This precision is appropriate for the current design, as we measure an overall scanning jitter of 4 nm (rms). If larger image fields are required, a lower magnification objective lens or galvanometers with larger mirrors can be employed.

The axial field curvature caused by the Quadscanner design is negligible because it is de-magnified with the square of the magnification factor. In our configuration, the field curvature amounts to about 25 nm across the whole image field. The chromatic magnification error at the image boundary is about 40 nm (633 nm vs. 775 nm) which is also negligible. If larger field sizes or a wider spectral range is desired, a correction may be necessary, which can be accomplished, e.g., by placing an additional $f = -1000$ mm silica lens between the objective lens and the tube lens.

2.3. Directional Beam Splitter (DBS)

The majority of biomedical investigations require the simultaneous imaging of multiple molecular species. The most straightforward way to address this demand is to use markers with different spectra. In STED microscopy, it is most desirable to use a single STED beam to inhibit multiple dyes together, which ensures that the co-localization errors are minimal. Therefore, all laser beams must be co-aligned and directed to the microscope while the emanating fluorescence must be separated and efficiently guided to the detectors. This becomes challenging when variable excitation wavelengths, e.g., from a supercontinuum, are used for excitation.

Excitation and fluorescence light are commonly separated with exchangeable dichroic beam splitters or with multiband beam splitters. However, mechanical exchange of beam splitters is susceptible to misalignment, and multiband beam splitters may sacrifice fluorescence. Additionally, filters with fixed spectral signatures severely limit the flexibility of fluorophore excitation provided by the supercontinuum laser source. Acousto-optical beam splitters are more versatile, because several wavelengths can be programmed, but their line width is limited to < 1 nm, which is why they lose efficiency when lasers with larger linewidths are used. They also introduce angular dispersion into the deflected beam. While this is negligible in confocal imaging, in STED microscopy it may compromise the doughnut minimum.

For these reasons we implemented a directional beam splitter (DBS) which separates beams by their propagation direction rather than by their wavelength [20]. Our DBS uses a Faraday rotator to separate the back-traveling fluorescence from the excitation and STED light propagating towards the sample. In essence, after having passed the polarizing beam splitter, the polarization of the excitation and the STED beams are rotated by the half-wave plate by 45° and subsequently rotated back by -45° so that they can pass the second polarizing beam splitter (Figure 4). The fluorescence part with the same polarization as the two laser beams travels back along the same path, but is finally deflected by the polarizing beam splitter facing the lasers; this is because the Faraday rotator and the halfwave plate

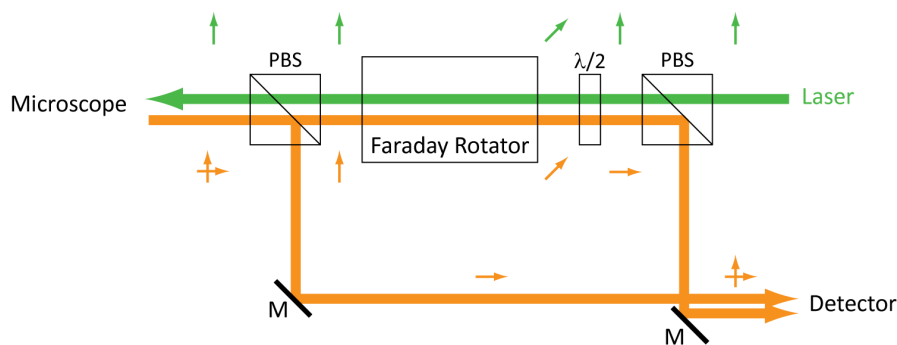


Figure 4. Schematic of the directional beam splitter (DBS). A Terbium Gallium Granate Faraday rotator is implemented to create a direction-dependent beam splitter. While light from the laser essentially passes the device unchanged, light traveling backwards to the laser (green) with the polarization direction of the laser becomes rotated by 90° and is coupled out by the polarizing beam splitter (PBS) at the laser port. The orthogonal polarization component of the (usually unpolarized) fluorescent light (orange) is coupled out at the polarizing beam splitter close to the microscope. The half wave retarder is not essential, but it allows keeping the beam path in a single plane. The two polarized detection beams may be recombined or detected by separate detectors as indicated in the schematic.

jointly rotate the field by a total of 90° . The polarization component of the fluorescence light that is orthogonal to the laser fields needs no rotation, since it can be readily coupled out before it reaches the Faraday rotator (see Figure 4). The two components may either be recombined or detected with separate detectors. We opted for the latter configuration, because it also offers measuring the anisotropy of the fluorescence emission.

The DBS exhibits a low spectral dependence caused by the dispersion of the Faraday rotator and the retarder plate. The transmission at the STED wavelength (775 nm) is $> 80\%$. The reflection efficiency for the fluorescence light (500–700 nm) towards the detectors is $> 90\%$ which is comparable to conventional dichroic beamsplitters (see Figure A3). Wider achromatic designs are conceivable with material mixes other than the off-the-shelf device used here. Residual reflections of the lasers which are also directed into the detection beam path by the DBS are sufficiently suppressed by the band pass filters in front of the detectors.

3. RESULTS

3.1. Resolution

The performance of the presented STED system was first tested using fluorescent beads with a nominal size of 20 nm excited at 630 nm. Crimson beads (Life Technologies) were immobilized on a coverslip using Poly-L-Lysine (SERVA Electrophoresis GmbH, Heidelberg, Germany). To determine the width of the fluorescence spot-like image rendered by a bead, a 2D-Gaussian model function was fitted to each bead image. On average, a full-width-half-maximum (FWHM) of 23 nm was found (see Figure A4). By deconvolution with the physical size of the beads (20 nm), the imaging resolution, in terms of the FWHM of the effective point-spread-function of the imaging modality was estimated as 19.5 nm.

We further imaged vimentin protein fibers in rat embryonic fibroblast cells (Figure 5), which were immunolabeled with primary and secondary antibodies conjugated to ATTO 647N (ATTO-TEC GmbH, Siegen, Germany). The measured diameters of the vimentin fibers in the STED image were ≤ 50 nm. This finding is consistent with model calculations assuming the true fiber diameter as 10 nm, the thickness of the attached antibody sandwich as ~ 16 nm and the resolution as 20–25 nm. Note that these numbers indicate the fact that the common immunofluorescence staining methods with primary and secondary antibodies are no longer appropriate at these resolution levels, because they significantly add up to the size of the feature to be imaged. Without the extension of the antibodies, the 10 nm fibers would appear only ~ 22 nm wide.

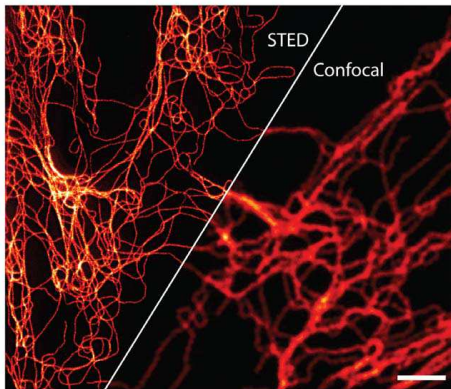


Figure 5. Confocal and STED image of vimentin stained with ATTO 647N. In the STED recording, the vimentin filaments appear with a diameter of ≤ 50 nm. The images are Wiener filtered for noise reduction without resolution enhancement. Scale bar: 2 μm .

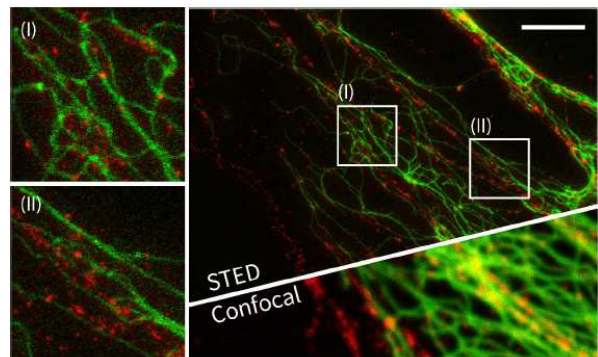


Figure 6. Dual staining of the proteins vimentin (labeled with CF680R, shown in green) and actinin (labeled with KK114, shown in red). Linear unmixing was applied to remove residual spectral crosstalk. Scale bar: 3 μm .

3.2. Multicolor Imaging

Many biomedical applications require the investigation of the proximity of two molecular species in order to investigate their interaction, i.e., co-localization studies. In widefield and confocal microscopy recording multiple colors is well established: different dyes are usually distinguished by their excitation and/or emission wavelengths. Selecting fluorophores for multicolor STED imaging has the additional boundary condition imposed by the STED wavelengths. Furthermore, care must be exerted that the STED beam does not significantly excite some of the dyes.

Until recently, multicolor STED microscopy approaches typically utilized multiple STED laser lines [21, 22]. Configurations with multiple excitation wavelengths and just a single wavelength for STED are preferable, because the common STED beam focal minimum defines the coordinate of emission for all fluorophores employed. Using a single STED doughnut for multiple fluorophores is possible in many cases, due to the rather broad and mutually overlapping emission spectra of many organic fluorophores at room temperature. Importantly, the use of a single STED laser line also avoids artifacts from residual chromatic shifts, giving highly reliable co-localization information.

If both the excitation and the emission spectra are overlapping, it is also possible to use just a single pair of excitation and STED wavelength for multiple fluorophores. The separation of the two is then accomplished by subtle differences in their emission spectra, such as shifts between their emission peaks. An example is given in Figure 6, where we show the proteins actinin and vimentin immunolabeled with the fluorophores KK 114 and CF 680R (Biotium, Inc., Hayward, CA, USA), respectively. The dyes and the pertinent features can be clearly separated. However, because CF 680R is slightly excited by the STED laser as well, producing ‘background’, we recorded a dedicated ‘background’ image by turning only the STED beam on and subtracting the ‘background’ image from the ordinary STED recording.

3.3. Fluorescence Lifetime Imaging

Because our microscope uses sub-nanosecond pulsed lasers, additional information about the fluorescence lifetime is available which can be used to further discriminate between multiple fluorophores [22]. This extra information does not impair the image brightness or noise levels. The electronics implemented here can be advantageously used for such lifetime-based multi-marker measurements. The synchronization of laser pulses and their correct relative timing is controlled with programmable delay lines in the FPGA device which also allows distributing the photons to several subsequent time bins, yielding a coarsely sampled photon counting histogram. From this histogram, one or more fluorescence lifetimes can be estimated.

In Figure 7 an image of a Vero cell is shown where beta-tubulin was immunolabeled with the fluorophore KK 114, whereas nup153 with the dye ATTO 647N. Both dyes were excited at 630 nm and de-activated by STED at 775 nm. The markers were distinguished just by their lifetimes which differed by 0.8 ns. Due to the similar spectral characteristics of the dyes, and because the same lasers are used for both fluorophores the images are free of chromatic misalignments.

The fluorescence lifetime τ of a single dye in each pixel can be estimated from this simplified formula [23]:

$$\tau = T_1 / \ln [(F_1 + F_2) / F_2] \quad (2)$$

where T_1 is the length of the first detection window, and F_1 , F_2 are the photon count numbers in detection window 1 and 2, respectively. The lifetime τ can be calculated with little computational effort and is therefore suitable for realtime display. However, the above formula disregards potential signal offset and the finite length of the second detection window. These simplifications are appropriate when lifetime differences or changes are to be monitored, as is the case here. For the separation of multiple markers absolute lifetimes are not of interest. The marker with the shorter lifetime dominates in the first window whereas the marker with the longer lifetime dominates in the second window, resembling data with spectral crosstalk. Therefore, the crosstalk can be removed with established linear unmixing methods [24–26]. An example of an image where three markers were separated by lifetime combined with excitation multiplexing is shown in Figure 8. Here actinin clusters and lamin are separated by fluorescence lifetime. Additionally, vimentin was separated by excitation multiplexing at 580 nm and 647 nm.

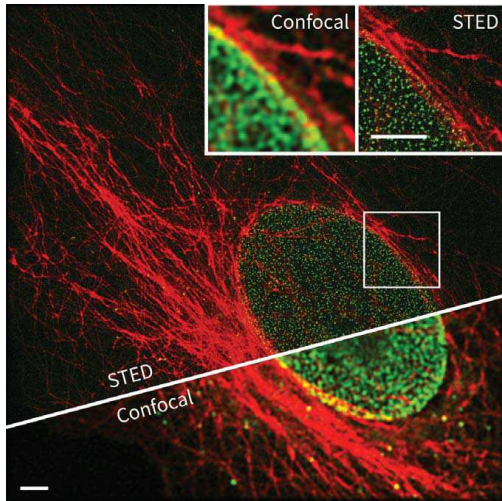


Figure 7. Fluorescence lifetime based channel separation using dual-gated detection. STED and confocal images of β -tubulin (immunolabeled with the fluorophore KK114, shown in red) and the nuclear pore complex (nup153 immunolabeled with ATTO 647N, shown in green) in a mammalian (vero) cell. The fluorescence lifetime of ATTO 647N is shorter by about 0.8 ns compared to KK114. The images were linearly unmixed and smoothed with a Wiener filter. Scale bars: 3 μ m.

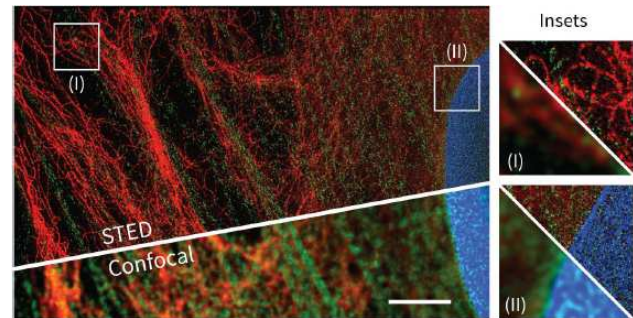


Figure 8. Three-color single-beam STED imaging with lifetime separation and excitation multiplexing (580 nm/647 nm). Cells were stained for vimentin (ATTO 590, shown in red), α -actinin (KK114, shown in green) and lamin (ATTO 647N, shown in blue). The images are smoothed with a Wiener filter. Scale bar: 2 μ m.

4. DISCUSSION AND CONCLUSION

We have described an integral optical design rendering a technically simple and inexpensive STED microscopy system. Fiber lasers, a novel achromatic beam splitting unit based on Faraday rotation, a birefringent wavefront modification unit, and an unconventional laser scanning scheme cooperatively reduce system complexity and alignment demands. Furthermore, by integrating most of the device control into a single reprogrammable FPGA board little additional electronics is required. All time-critical tasks such as laser pulse synchronization and time-gated photon detection can be performed on this board. Group velocity dispersion in the optical fiber of the supercontinuum laser, which may cause variable delays for different excitation wavelengths is also compensated in the FPGA program. New functionality can be easily added in the software.

In polymer nanoparticle samples, this rugged arrangement displayed a resolution of ~ 20 nm whereas in biological samples the resolution was ~ 30 nm. Note that the attained resolution is primarily a function of the fluorophores employed, which is, of course, inherent to a concept separating features via molecular states. The maximum resolution attainable with a particular fluorophore and STED wavelength depends on the characteristic intensity I_s and the maximum applicable doughnut intensity I . The demonstration of a specific resolution value (here 20 nm) with polymer nanoparticles proves that the setup meets the optical conditions for attaining this value.

True co-localization of different target structures was achieved by lifetime separation of fluorescent labels that were spectrally similar. Because the same excitation and STED wavelengths were used for two dyes and the channels were recorded simultaneously, the co-localization is free of chromatic aberrations or drift. Time-gated detection is useful in many regards. Early photons, i.e., those emitted within the first few 100 ps after the excitation pulse, carry little or no superresolution information because, at this instant, the STED pulse has not efficiently deactivated the fluorophores located at the focal periphery. Discarding these early photons by time-gating therefore results in a much improved

image quality.

As this development is continuing, even more rugged and more compact systems can be anticipated, especially when microscope suppliers adopt such design strategies. For example, the easySTED wave plate could be built into the objective lens itself (as in Zernike's phase contrast microscopy) because the actual functional element is only a few hundred microns thick. Commercial monolithic opto-mechanical designs have the potential to further improve the ruggedness of the system. The cost level of the system design presented here is already below current multipurpose confocal fluorescence microscopes, which should make direct and push-button far-field fluorescence microscopy with resolution down to 20 nm a standard laboratory tool in the near future.

APPENDIX A. SUPPLEMENTARY INFORMATION

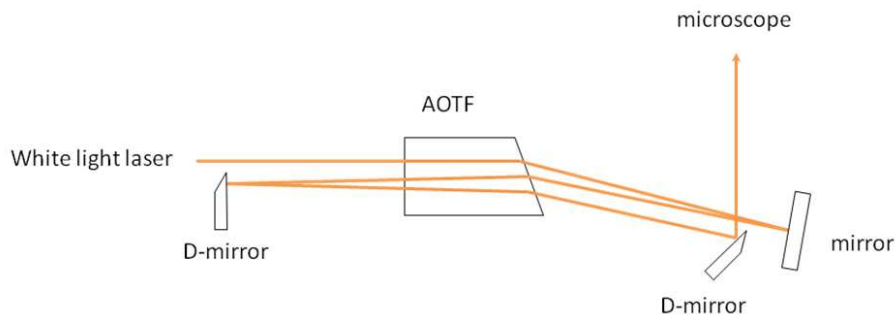


Figure A1. In the triple pass AOTF arrangement the selected beam is diffracted three times by the sound wave in the crystal, and as such improves the suppression of unwanted spectral parts of the supercontinuum source (white light laser). The zero order beams of all passes are blocked (not shown).

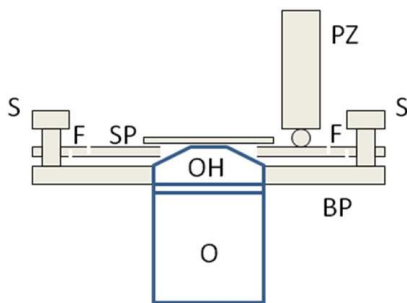


Figure A2. Schematic of the objective mounted stage. The base plate (BP) is clamped directly at the objective head (OH) of the objective (O). The height of the sample holder plate (SP) on top of the base plate can be coarsely adjusted by fine threaded screws (S). The sample holder is connected to the holder with flexure bearings which allow fine focusing and z-scanning with a piezo (PZ).

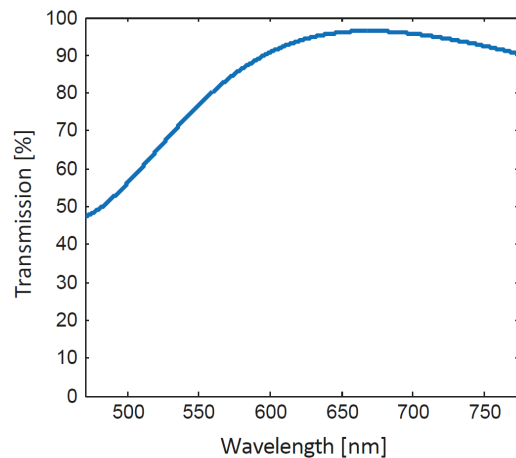


Figure A3. The transmission of the directional beam splitter (DBS) for the fluorescence light between 600 and 750 nm is above 90%; shown is the fit curve of the sum of both polarizations.

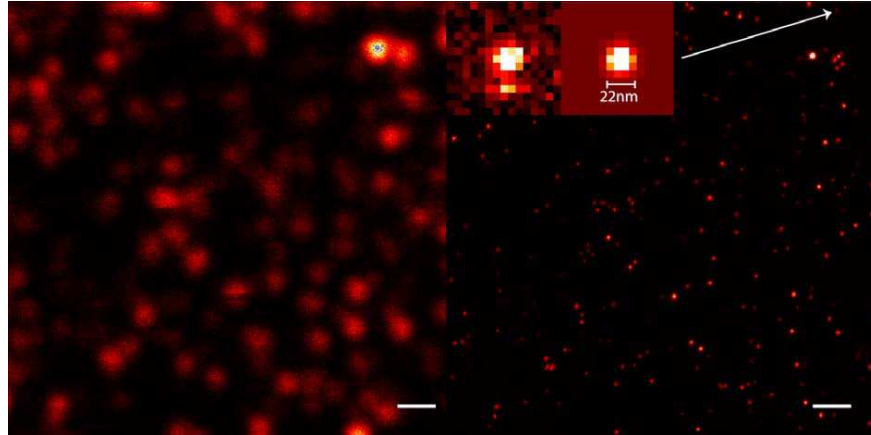


Figure A4. Resolution measurement with 20 nm sized fluorescent beads. Beads are image at a size of $23.1 \text{ nm} + / - 5.5 \text{ nm}$ ($N = 10$). The size was measured by fitting a Gaussian model intensity distribution to the spots. The inset shows an example bead with the corresponding fitted intensity. Image size: $5.8 \mu\text{m} \times 5.8 \mu\text{m}$, pixel size: $5 \text{ nm} \times 5 \text{ nm}$, dwell time: $100 \mu\text{s}$, excitation pulse: 31.2 pJ/pulse , $\lambda = 630 \text{ nm}$, pulse length: 100 ps , STED pulse: 6.91 nJ/pulse , $\lambda = 775 \text{ nm}$, pulse length: 1.2 ns , repetition rate: 38.6 MHz , STED pulse delay: 0.7 ns , detection gate: $2\text{--}12 \text{ ns}$ (after excitation pulse). Scale bar: 500 nm .

ACKNOWLEDGMENT

We acknowledge the Federal Ministry of Education and Research (BMBF) for funding this work within the project STEDlight (FKZ: 13N11173).

REFERENCES

1. Hell, S. W. and J. Wichmann, "Breaking the diffraction resolution limit by stimulated-emission — Stimulated-emission-depletion fluorescence microscopy," *Optics Letters*, Vol. 19, No. 11, 780–782, 1994.
2. Klar, T. A., et al., "Fluorescence microscopy with diffraction resolution barrier broken by stimulated emission," *Proceedings of the National Academy of Sciences of the United States of America*, Vol. 97, No. 15, 8206–8210, 2000.
3. Westphal, V. and S. W. Hell, "Nanoscale resolution in the focal plane of an optical microscope," *Physical Review Letters*, Vol. 94, 143903, 2005.
4. Hell, S. W., "Toward fluorescence nanoscopy," *Nature Biotechnology*, Vol. 21, No. 11, 1347–1355, 2003.
5. Hell, S. W. and M. Kroug, "Ground-state depletion fluorescence microscopy, a concept for breaking the diffraction resolution limit," *Applied Physics B: Lasers and Optics*, Vol. 60, 495–497, 1995.
6. Hell, S. W., S. Jakobs, and L. Kastrup, "Imaging and writing at the nanoscale with focused visible light through saturable optical transitions," *Applied Physics A: Materials Science & Processing*, Vol. 77, 859–860, 2003.
7. Rust, M. J., M. Bates, and X. W. Zhuang, "Sub-diffraction-limit imaging by stochastic optical reconstruction microscopy (STORM)," *Nature Methods*, Vol. 3, 793–795, 2006.
8. Betzig, E., et al., "Imaging intracellular fluorescent proteins at nanometer resolution," *Science*, Vol. 313, 5793, 1642–1645, 2006.
9. Hess, S. T., T. P. K. Girirajan, and M. D. Mason, "Ultra-high resolution imaging by fluorescence photoactivation localization microscopy," *Biophysical Journal*, Vol. 91, No. 11, 4258–4272, 2006.
10. Dertinger, T., et al., "Two-focus fluorescence correlation spectroscopy: A new tool for accurate and absolute diffusion measurements," *Chem. Phys. Chem.*, Vol. 8, No. 3, 433–443, 2007.

11. Hell, S. W., “Far-field optical nanoscopy,” *Science*, Vol. 316, No. 5828, 1153–1158, 2007.
12. Willig, K. I., et al., “STED microscopy with continuous wave beams,” *Nature Methods*, Vol. 4, No. 11, 915–918, 2007.
13. Voloshinov, V. B., L. N. Magdich, and G. A. Knyazev, “Tunable acousto-optic filters with the multiple interaction of light and sound,” *Quantum Electronics*, Vol. 35, No. 11, 1057–1063, 2005.
14. Göttfert, F., et al., “Coaligned dual-channel STED nanoscopy and molecular diffusion analysis at 20 nm resolution,” *Biophysical Journal*, Vol. 105, No. 1, L01–L03, 2013.
15. Moffitt, J. R., C. Osseforth, and J. Michaelis, “Time-gating improves the spatial resolution of STED microscopy,” *Optics Express*, Vol. 19, No. 5, 4242–4254, 2011.
16. Vicidomini, G., et al., “STED nanoscopy with time-gated detection: theoretical and experimental aspects,” *PLoS One*, Vol. 8, No. 1, e54421 (1–12), 2013.
17. Wildanger, D., et al., “A STED microscope aligned by design,” *Optics Express*, Vol. 17, No. 18, 16100–16110, 2009.
18. Reuss, M., J. Engelhardt, and S. W. Hell, “Birefringent device converts a standard scanning microscope into a STED microscope that also maps molecular orientation,” *Optics Express*, Vol. 18, No. 2, 1049–1058, 2010.
19. Bingen, P., et al., “Parallelized STED fluorescence nanoscopy,” *Optics Express*, Vol. 19, No. 24, 23716–23726, 2011.
20. Schreiber, F., *Device and Method for Distributing Illumination Light and Detection Light in a Microscope*, 2013.
21. Donnert, G., et al., “Two-color far-field fluorescence nanoscopy,” *Biophysical Journal*, Vol. 92, No. 8, L67–L69, 2007.
22. Bückers, J., et al., “Simultaneous multi-lifetime multi-color STED imaging for colocalization analyses,” *Optics Express*, Vol. 19, No. 4, 3130–3143, 2011.
23. Salthouse, C. D., R. Weissleder, and U. Mahmood, “Development of a time domain fluorimeter for fluorescent lifetime multiplexing analysis,” *IEEE Transactions on Biomedical Circuits and Systems*, Vol. 2, No. 3, 204–211, 2008.
24. Demandolx, D. and J. Davoust, “Multicolour analysis and local image correlation in confocal microscopy,” *Journal of Microscopy-Oxford*, Vol. 185, 21–36, 1997.
25. Dickinson, M. E., et al., “Multi-spectral imaging and linear unmixing add a whole new dimension to laser scanning fluorescence microscopy,” *Biotechniques*, Vol. 31, No. 6, 1272, 2001.
26. Neher, R. A., et al., “Blind source separation techniques for the decomposition of multiply labeled fluorescence images,” *Biophys. J.*, Vol. 96, No. 9, 3791–3800, 2009.